THE JOURNAL OF BIOLOGICAL CHEMISTRY VOL. 290, NO. 9, pp. 5592–5605, February 27, 2015

Glycogen Synthase Kinase-3 (GSK3) Inhibition Induces Prosurvival Autophagic Signals in Human Pancreatic Cancer Cells*

Received for publication, October 3, 2014, and in revised form, December 12, 2014 Published, JBC Papers in Press, January 5, 2015, DOI 10.1074/jbc.M114.616714

Benoît Marchand[‡], Dominique Arsenault[‡], Alexandre Raymond-Fleury[‡], François-Michel Boisvert[§1], and Marie-Josée Boucher[‡1,2]

From the [‡]Department of Medicine, Gastroenterology Division, and the [§]Department of Anatomy and Cell Biology, Faculté de Médecine et des Sciences de la Santé, Pavillon de Recherche Appliquée sur le Cancer, Université de Sherbrooke, Sherbrooke, Québec J1E 4K8, Canada

Background: Glycogen synthase kinase-3 (GSK3) inhibition promotes apoptosis of pancreatic cancer cells.
Results: GSK3 inhibition concomitantly triggers a prosurvival autophagic response.
Conclusion: Autophagy inhibition promotes GSK3 inhibition-induced apoptosis.
Significance: GSK3 has a dual role in pancreatic cancer cell survival.

Glycogen synthase kinase-3 (GSK3) are ubiquitously expressed serine-threonine kinases involved in a plethora of functions ranging from the control of glycogen metabolism to transcriptional regulation. We recently demonstrated that GSK3 inhibition triggers JNK-cJUN-dependent apoptosis in human pancreatic cancer cells. However, the comprehensive picture of downstream GSK3-regulated pathways/functions remains elusive. Herein, counterbalancing the death signals, we show that GSK3 inhibition induces prosurvival signals through increased activity of the autophagy/lysosomal network. Our data also reveal a contribution of GSK3 in the regulation of the master transcriptional regulator of autophagy and lysosomal biogenesis, transcription factor EB (TFEB) in pancreatic cancer cells. Similarly to mammalian target of rapamycin (mTOR) inhibition, GSK3 inhibitors promote TFEB nuclear localization and leads to TFEB dephosphorylation through endogenous serine/threonine phosphatase action. However, GSK3 and mTOR inhibition impinge differently and independently on TFEB phosphorylation suggesting that TFEB is regulated by a panel of kinases and/or phosphatases. Despite their differential impact on TFEB phosphorylation, both GSK3 and mTOR inhibitors promote 14-3-3 dissociation and TFEB nuclear localization. Quantitative mass spectrometry analyses further reveal an increased association of TFEB with nuclear proteins upon GSK3 and mTOR inhibition suggesting a positive impact on TFEB transcriptional function. Finally, a predominant nuclear localization of TFEB is unveiled in fully fed pancreatic cancer cells, whereas a reduction in TFEB expression significantly impairs their capacity for growth in an anchorage-independent manner. In addition, TFEB-restricted cells are more sensitive to apoptosis upon GSK3 inhibition. Altogether, our data uncover new functions under the control of GSK3 in pancreatic cancer cells in addition to providing key insight into TFEB regulation.

Pancreatic ductal adenocarcinoma (PDAC)[3] is the 4th leading cause of cancer-related deaths worldwide and the only malignancy with a 5-year survival rate in the single digits, *i.e.* 6% (1–3). These statistics have not improved over the last 40 years and although identification of the most frequently mutated genes in PDAC (*KRAS*, *P53*, *P16*, and *SMAD4*) have provided important insights into PDAC pathogenesis (4), they have not led to improvement in either diagnosis or treatment. Consequently, PDAC is still diagnosed at advanced stages and is highly resistant to current chemotherapeutic agents (1–3). Finding the Achilles heel of pancreatic cancer cells and/or new therapeutic options to sensitize these cells to chemotherapeutic agents is imperative in the quest to improve the fate of PDAC patients.

We and others have previously demonstrated that inhibition of glycogen synthase kinase-3 (GSK3) impairs pancreatic cancer cell growth (5–10) thus providing a rationale for assessing the potential clinical utility of GSK3 inhibitors in PDAC patients (11). Notably, we have shown that GSK3 inhibition triggers apoptosis by mechanisms involving JNK-cJUN activation (8), whereas others have observed reduced growth as a result of NF-κB activity down-regulation (5, 7, 9, 10, 12). Despite the general consensus supporting an important role for GSK3 in the maintenance of pancreatic cancer cell growth, a comprehensive picture of the underlying downstream GSK3 effectors remains elusive. A better understanding of these effec-

* This work was supported in part by Natural Sciences and Engineering Research Council of Canada Grant NSERC 341809 and Canadian Institutes of Health Research Grant MOP-106456 (to M. J. B.).

[1] Scholars from the Fonds de Recherche Santé Québec (FRQ-S) and members of the FRQ-S-funded Centre de recherche du Centre hospitalier universitaire de Sherbrooke (CRCHUS).

[2] To whom correspondence should be addressed: Université de Sherbrooke, 3201 rue Jean Mignault, Sherbrooke, P.Q., J1E 4K8, Canada. Tel.: 819-821-8000 (ext. 72793); Fax: 819-820-6831; E-mail: marie-josee.boucher@usherbrooke.ca.

[3] The abbreviations used are: PDAC, pancreatic ductal adenocarcinoma; GSK3, glycogen synthase kinase-3; HPDE, human pancreatic ductal epithelial cells; MEF, mouse embryonic fibroblasts; PARP, poly(ADP)-ribose polymerase; TFEB, transcription factor EB; LC3B, microtubule-associated protein 1 light chain 3B; L, M, and H, light, medium, and heavy; DMSO, dimethyl sulfoxide; mTOR, mammalian target of rapamycin.

tors is crucial before proposing GSK3 inhibitors as a therapeutic alternative in the clinical setting of PDAC patients.

Few studies have recently uncovered a regulation of autophagy by GSK3 inhibitors although the outcome on autophagy and/or cell viability appeared context-dependent (13–15). Macroautophagy (referred herein as autophagy) is a catabolic process used by cells to degrade long-lived proteins and cytoplasmic components by delivering the latter to lysosomes (16, 17). The resulting metabolites can be reused as sources of energy or for the synthesis of new macromolecules (18). The role of autophagy in tumorigenesis is complex displaying both tumor suppressive and tumor promoting roles (19–25). Recently, human pancreatic tumors and pancreatic cancer cell lines were characterized for their high levels of basal autophagy (26). As a result, inhibition of autophagy considerably impaired their growth *in vitro* and *in vivo* suggestive of a critical dependence of pancreatic cancer cells on autophagy (26). Furthermore, anticancer drugs such as gemcitabine and 5-fluorouracil were shown to further enhance autophagy, albeit with some groups reporting a cytotoxic role (27, 28), whereas others suggested a cytoprotective role (29–31) for autophagy. Thus, the contribution of autophagy in the viability and/or growth of human pancreatic cancer cells warrants further investigation.

Herein, we further characterized the impact of GSK3 inhibition in pancreatic cancer cells. While inducing JNK-dependent apoptotic markers (8), GSK3 inhibition was found to promote a distinct autophagic response independently of the JNK-cJUN pathway. Preventing this autophagic response resulted in sensitization of cells to apoptosis suggesting a prosurvival role for autophagy upon GSK3 inhibition. Treatment with GSK3 inhibitors rapidly led to the dephosphorylation and nuclear localization of transcription factor EB (TFEB) recently identified as a master regulator of autophagy and lysosomal biogenesis. Moreover, TFEB-depleted pancreatic cancer cells displayed increased sensitivity to apoptosis upon treatment with GSK3 inhibitors providing support for a role for TFEB in the prosurvival signals induced by GSK3 inhibitors.

EXPERIMENTAL PROCEDURES

Cell Culture and Drug Treatments—HEK293T cells and human pancreatic cancer cells PANC1 and MIA PaCa-2 (American Type Culture Collection) were grown in DMEM supplemented with 10% fetal bovine serum (FBS) (Wisent, 095150), 2 mM Glutamax (Invitrogen, 35050-61) in a humidified 5% CO_2 atmosphere at 37 °C (8). The non-transformed human pancreatic ductal epithelial cell line (HPDE) was kindly provided by M. S. Tsao (University of Toronto) and cultured as described in keratinocyte/serum-free medium (Invitrogen, 17005-042) (8, 32, 33). The stable populations of PANC1-shCTL and PANC1-shcJUN cells were previously described (8). Mouse embryonic fibroblast (MEF) cell lines isolated from *Gsk3β*$^{-/-}$ mouse embryo and wild-type (*Gsk3β*$^{+/+}$) littermates were established in culture as immortal cell lines and were kindly provided by J. R. Woodgett (The Lunenfeld-Tanenbaum Research Institute, Toronto) (34). MEF were maintained in DMEM supplemented with 10% FBS and 2 mM Glutamax. Cells were incubated for the indicated time period with GSK3 inhibitors CHIR99021 (Selleckchem, S2924) or SB216763 (Tocris, 1616). When indicated, cells were incubated with the JNK inhibitor SP600125 (EMD Millipore, 420128), the mTOR inhibitor Torin1 (Selleckchem, S2827), or the S6K1 inhibitor PF-4708671 (Selleckchem, S2163). For evaluation of autophagic flux, cells were incubated with chloroquine (Sigma) or Bafilomycin A1 (LC Laboratories, B-1080). To inhibit autophagy, cells were incubated with the vacuolar H^+-ATPase inhibitor Bafilomycin A1. To inhibit endogenous serine/threonine phosphatases, cells were preincubated for 15 min with Calyculin A (Cell Signaling Technology, 9902) prior to CHIR99021 or Torin1 addition. The *pan*-caspase inhibitor caspase inhibitor I (EMD Millipore, 627610) was used to inhibit caspase activation.

Antibodies—The following antibodies were used: anti-cJUN, anti-ERK1, anti-GFP, anti-LAMIN B (Santa Cruz Biotechnology, sc-1694, sc-93, sc-9996, and sc-6217, respectively), anti-14-3-3, anti-phospho-Ser 14-3-3 binding motif, anti-ATG5, anti-BECLIN-1, anti-cleaved CASPASE 7, anti-phospho-cJUN, anti-phospho-ERK1/2, anti-GAPDH, anti-GSK3 α/β, anti-LC3B, anti-cleaved PARP, anti-PARP, anti-S6K1, anti-phospho-S6K1, anti-TFEB (Cell Signaling Technology, 8312, 9606, 2630, 3738, 9491, 9261, 9101, 2118, 5676, 3868, 9541, 9542, 2708, 9234, 4240 respectively), and anti-ACTIN (Millipore, MAB1501). Horseradish peroxidase (HRP)-conjugated anti-mouse and anti-rabbit IgG were from Jackson Immunoresearch Laboratories (115-035-003 and 111-035-003). HRP-conjugated anti-goat IgG was from Santa Cruz Biotechnology (sc-2953). Alexa Fluor 488-conjugated donkey anti-rabbit IgG was used (Molecular Probes, 21206).

Immunoblotting and Immunoprecipitation—Cells were washed with ice-cold PBS, then lysed in either Triton buffer (1% Triton X-100, 50 mM Tris, pH 7.5, 100 mM NaCl, 5 mM EDTA, 0.2 mM orthovanadate, 40 mM β-glycerophosphate, 50 mM NaF, 10% glycerol, 1 mM PMSF, 0.5 μg/ml of aprotinin, 0.5 μg/ml of leupeptin, and 0.7 μg/ml of pepstatin) or high salt lysis buffer (1% Nonidet P-40, 50 mM Tris, pH 7.5, 300 mM NaCl, 150 mM KCl, 5 mM EDTA, 10 mM NaF, 10% glycerol, 0.2 mM orthovanadate, 1 mM PMSF, 0.5 μg/ml of aprotinin, 0.5 μg/ml of leupeptin, and 0.7 μg/ml of pepstatin) followed by a 5-s sonication. Total cell lysates were cleared of cellular debris by centrifugation (10,000 × *g*, 10 min, 4 °C). Protein concentrations were measured using the bicinchronic acid (BCA) reagent procedure from Pierce (23225) with bovine serum albumin as standard. Equal amounts of protein were separated by SDS-PAGE, and proteins were detected immunologically after electrotransfer onto nitrocellulose or polyvinylidene difluoride membranes as previously described (8). For immunoprecipitation, 1.5 mg of cleared lysates were incubated with 15 μl of GFP-Trap-agarose beads (Chromotek, gta) for 2 h at 4 °C under agitation. The beads were then washed three times with lysis buffer before boiling for 5 min in 4× Laemmli sample buffer (×1 = 62.5 mM Tris-HCl, pH 6.8, 2.3% SDS, 10% glycerol, 1 mM PMSF, 0.005% bromphenol blue, and 5% β-mercaptoethanol).

Subcellular Fractionation—Cells were washed twice with ice-cold PBS, lysed in Buffer A (10 mM Hepes, pH 7.9, 10 mM KCl, 0.1 mM EDTA, 0.1 mM EGTA, 1 mM DTT, 10 mM NaF, 10 mM β-glycerophosphate, 200 μM orthovanadate, 1 mM PMSF, 0.5 μg/ml of aprotinin, 0.5 μg/ml of leupeptin, and 0.7 μg/ml of pepstatin) and kept on ice for 15 min after which Nonidet P-40

(0.625%) was added. The lysates were vortexed 15 s before being centrifuged at 12,000 × *g* for 30 s at 4 °C. The supernatants containing the cytoplasmic proteins were collected. The pellets were resuspended in Buffer B (20 mM Hepes, pH 7.9, 0.4 M NaCl, 1 mM EDTA, 1 mM EGTA, 1 mM DTT, 10 mM NaF, 10 mM β-glycerophosphate, 5% glycerol, 200 μM orthovanadate, 1 mM PMSF, 0.5 μg/ml of aprotinin, 0.5 μg/ml of leupeptin, and 0.7 μg/ml of pepstatin) and centrifuged at 10,000 × *g*, for 10 min at 4 °C. The supernatants representing the nuclear proteins were collected. Protein concentration was measured with the BCA reagent and samples were analyzed by immunoblotting.

Lysosome Labeling—Lysosomes were visualized by incubating cells with the Lysotracker® Red DND-99 dye (50 nM) (Molecular Probes; L-7528) for 1 h at 37 °C 5% CO_2. Cells were fixed in 2% paraformaldehyde (30 min, 4 °C), washed with PBS, stained with 4′,6-diamidino-2-phenylindole (DAPI) for 5 min, washed again, and visualized under laser excitation at 555 nm.

Immunofluorescence Confocal Microscopy—Cells were seeded at 70% confluence on glass coverslips. The coverslips were placed in 6-well culture plates and incubated for 24 h. Cells were then treated for 1 h with vehicle (DMSO), CHIR99021 (5 μM), or Torin1 (250 nM). Following incubations, the cells were washed with PBS, fixed with 2% paraformaldehyde (30 min, 4 °C), permeabilized (0.1% Triton X-100 or 100% methanol), and immunostained for 2 h with the primary antibody. The cells were washed and incubated with Alexa 488-conjugated secondary antibody for 1 h. Cells were then stained with DAPI for 5 min. The cells were washed again followed by slide mounting using Immu-Mount (Thermo Scientific, 9990402). Cells were examined with a Zeiss LSM700 confocal microscope equipped with ×20, 63, and 100 oil immersion objectives or an Olympus FV1000 confocal microscope equipped with a ×63 oil immersion objective. Specimens were laser-excited sequentially at 488 and 405 nm. Serial horizontal optical sections of 512 × 512 pixels with 2-times line averaging were taken at 0.4-μm intervals through the entire thickness of the cell. Images were acquired on the same day, typically from 15 cells of similar size from each experimental condition, under identical settings. Stack images of 5 to 6 (×20), 7 to 9 (×63), or 15 to 18 (×100) slices are shown.

Image Analysis and Quantitative Measurement—In the case of Alexa 488/DAPI-merged fluorescence images, dot fluorograms were obtained by plotting pixel values of each marker in the vertical and horizontal axes, respectively. Thresholds were determined using single markers followed by noise and background subtraction. Quadrant markers were adjusted forming background (C), green-only (D), blue-only (A), and co-localization areas (B). The percentage of colocalization was calculated as: (B)/((B)+(D)) × 100. To determine fluorescence quantification, images were processed for a total of 15 slices per cell on 15 size-matched cells for each experimental condition, with experiments performed at least twice. Images are shown in pseudocolor, according to their original fluorochromes, merged (FluoView software (Olympus)), then cropped and assembled with Adobe Photoshop software. For calculation of the percentage of nuclear TFEB-labeled cells, cells were prepared as described above. Cells were visualized by fluorescence microscopy, and cells with nuclear TFEB were identified by the colocalization between nucleus (DAPI) and TFEB (Alexa 488) staining, and counted. Six fields of 50 cells were counted for each experimental condition.

Transfections—Cells were transfected with Lipofectamine 2000 (Invitrogen, 11668-019) or Effectene (Qiagen, 301425) according to the manufacturer's recommendations and as previously described (8). For small interfering RNA (siRNA)-mediated silencing, PANC1 cells were transfected with 100 nM of a control siRNA (Dharmacon, D-001210-03-05) or an ATG5 siRNA (Santa Cruz Biotechnology, sc-41445). Twenty-four hours post-transfection, cells were treated with CHIR99021 or vehicle (DMSO) prior to protein expression analysis by immunoblotting. For the expression of TFEB-EGFP, HEK293T and PANC1 cells were transfected for 48 h with the pEGFP-N1-TFEB construct (Addgene plasmid 38119) followed by 1 h treatment with vehicle (DMSO), CHIR99021, or Torin1. Cells were either lysed for protein expression analysis by immunoblotting or processed for immunofluorescence confocal microscopy.

Generation of Lentiviruses and Infection—The non-target (Sigma, SHC-16), GSK3β (Sigma; TRCN0000040001), GSK3α (Sigma; TRCN0000039766), and TFEB (OpenBioSystems; TRCN0000013111) targeting lentiviral short hairpin RNA (shRNA) expression vectors were used. Lentiviruses were produced in HEK293T and used for PANC1 infection as previously described (8). For the generation of stable PANC1-shnon-target (shCTL) and PANC1-shTFEB populations, infected cells were selected (10 days) and maintained in puromycin (5 μg/ml).

Soft Agarose Assay—Anchorage-independent growth was tested as previously described (8). Briefly, 6-well dishes were precoated with 1.5 ml/well mixture (1:1) of 2× DMEM without phenol red and agarose type VII 1.4% (Sigma, A9045). Cells were then seeded on top of the precoated wells by adding 2 ml of DMEM/agarose mixture (1:1) containing 7,500 cells/ml, after which the plates were allowed to solidify. For treatments, fresh 1× DMEM without phenol red supplemented with 10% FBS containing the specified inhibitors was added to the surface of the agarose and changed daily. After 3 weeks, colonies were stained by adding 500 μl of 3-(4,5-dimethylthiazol-2-yl)-2,5-diphenyltetrazolium bromide (Calbiochem, 475989) at 0.5 mg/ml in PBS to the surface of the agarose and incubated for 3 h at 37 °C in 5% CO_2. Images were acquired and colonies were counted using ImageJ software version 1.47d.

Stable Isotope Labeling and Mass Spectrometry Analysis—HEK293T cells were grown for at least 6 passages in DMEM lacking arginine and lysine (Invitrogen, A14431-01) supplemented with 10% dialyzed FBS (Invitrogen, 26400-044), 2 mM L-Glutamax, 100 units/ml of penicillin/streptomycin (Wisent, 450-201-EL), and either light arginine and lysine (LIGHT condition) (Arg^0, Lys^0; Sigma A5006, L5501), medium arginine and lysine (MEDIUM condition) (Arg^6, Lys^4; Cambridge Isotope Laboratories CNM-2265, DLM-2640), or heavy arginine and lysine (HEAVY condition) (Arg^{10}, Lys^8; Cambridge Isotope Laboratories CNLM-539, CNLM-291) prior to transfection and immunoprecipitation experiments. HEK293T cells grown in Light (L), Medium (M), or Heavy (H) conditions were seeded in 15-cm dishes. The following day, cells in M and H conditions were transfected with 5 μg/dish of the EGFP-N1-TFEB plas-

mid. Twenty-four hours post-transfection, the transfected cells in the H condition were treated for 1 h with either CHIR99021 or Torin1, whereas the cells in M condition were treated with DMSO. Hence, cells in the L condition represented control nontransfected/untreated cells, cells in the M condition represented TFEB-EGFP-transfected DMSO-treated cells, and cells in the H condition represented TFEB-EGFP-transfected and treated (either with CHIR99021 or Torin1) cells. Cells from all conditions were lysed and TFEB-EGFP was immunoprecipitated from 5 mg of protein lysates using 50 μl of GFP-Trap-agarose beads (ChromoTek, gta) at 4 °C for 2 h. Prior to on-beads trypsin digestion, samples from L, M, and H conditions were combined at a 1:1:1 ratio and washed 5 times in 20 mM ammonium bicarbonate. Proteins were reduced in 10 mM DTT for 30 min at 60 °C and then alkylated by adding 15 mM iodoacetamide for 1 h at room temperature. Iodoacetamide was quenched by increasing DTT concentration to 15 mM and on-beads digestion was performed with 1 μg of trypsin gold (Promega, V5280) overnight at 37 °C. The digestion was stopped by acidifying to 1% formic acid and the supernatants were transferred to LoBind tubes (Eppendorf, 13-698-794). The beads were resuspended in a 60% acetonitrile, 0.1% formic acid solution for 5 min and the supernatant was combined with the previous supernatant. Samples were then lyophilized in a SpeedVac and resuspended in 20 μl of 0.1% trifluoroacetic acid. Desalting and concentration of sample peptides was carried out using ZipTip (Millipore, ZTC18S096) according to the manufacturer's recommendations. Peptides were resuspended in 25 μl of 1% formic acid and separated on-line with an Easy nLC system (Thermo Fisher Scientific). Samples (5 μl) were loaded as described (35). Peptides were eluted with a gradient from 10 to 60% solvent B over 240 min with a constant flow of 250 nl/min. The high-performance liquid chromatography (HPLC) system was coupled to a QExactive Orbitrap mass spectrometer (Thermo Fisher Scientific) through a nanoscale LC interface (Dionex Ultimate 3000; Thermo Fisher Scientific). The spray voltage was 2 kV, and the temperature of the heated capillary was 270 °C. Survey full-scan spectra (mass/charge ratio (m/z) = 350 to 1600) were acquired in positive ion mode with a resolution of 70,000 at m/z = 400 after accumulation of 1,000,000 ions. Up to 10 most-intense ions were sequenced by higher energy collisional dissociation in the Orbitrap. Precursor ion charge-state screening was enabled, and all unassigned charge states as well as 1, 7, 8, and >8 charged peptides were rejected. The dynamic exclusion list was restricted to a maximum of 500 entries with a maximum retention period of 40 s and a relative mass window of 10 parts per million (ppm). Orbitrap measurements were performed, enabling the lock mass option for survey scans to improve mass accuracy. Data were acquired with the Xcalibur software (version 2.1). Quantification was performed using the MaxQuant software (version 1.4.1.2) and data were searched using Andromeda against the Uniprot human protein database. The initial mass tolerance was set to 20 ppm and MS/MS tolerance was 0.5 Da. The carbamidomethylation of cysteines was set as a fixed modification. The false discovery rate was set to 0.01 and the minimum peptide length required was set to 7 residues.

Data Presentation and Statistical Analysis—All experiments were performed independently at least three times. Typical immunoblots are shown. Densitometric analyses were performed using ImageJ software version 1.47d. Data were analyzed by Prism 6 (GraphPad Prism) by unpaired t test. Results are expressed as means and error bars represent S.E. Differences were considered statistically significant when $p < 0.05$.

RESULTS

GSK3 Inhibition Induces an Autophagic Response in Human Pancreatic Cancer Cells—To evaluate the impact of GSK3 inhibitors on autophagy, we first analyzed expression levels of the microtubule-associated protein 1 light chain 3B II (LC3B II), a LC3B-phosphatidylethanolamine conjugate and autophagosomal marker (16, 17). Treatment of pancreatic cancer cells with GSK3 inhibitors CHIR99021 and SB216763 (8) induced PARP and CASPASE 7 cleavages but also led to increased expression of LC3B II, indicative of an autophagic response (Fig. 1*A*). Similar results were obtained in GSK3β-depleted cells, *i.e.* reduction of GSK3β expression led to increased PARP and CASPASE 7 cleavages (8) and increased expression of LC3B II (see Figs. 1*C* and 3*B*). To ensure that the increased LC3B II expression reflected an increase of autophagy and not a blockade of autophagosome degradation, autophagic flux was examined. Inhibition of autophagosome degradation by chloroquine further enhanced LC3B II expression upon treatment with GSK3 inhibitor (Fig. 1*B*) or in cells transduced with a shRNA targeting GSK3β (Fig. 1*C*) suggesting that GSK3 inhibition promotes an autophagic response in pancreatic cancer cells. Noteworthy, the induction of autophagy, visible at 24 h post-treatment, preceded the detection of apoptotic markers (Fig. 1*A*). To further support the induction of autophagy upon treatment with GSK3 inhibitors, autophagosome formation (punctate LC3B) was examined using confocal microscopy. As shown in Fig. 1*D*, LC3B puncta were detected in DMSO-treated (control) pancreatic cancer cells suggestive of a high degree of autophagy in these cells. This observation is in agreement with a previous report demonstrating an elevated level of autophagy in human pancreatic cancer cell lines that is required for their growth (26). Despite the high level of basal autophagy, an increased staining of LC3B puncta per cell was observed upon treatment with CHIR99021 or the mTOR inhibitor Torin1 (Fig. 1*D*), the latter being used as a known inducer of autophagy (16, 17). For completion of autophagy, the autophagosomes ultimately fuse with lysosomes to ensure the degradation of autophagosomal content (16, 17, 36). We therefore examined the lysosomal system by performing labeling of these organelles with Lysotracker. Both GSK3 and mTOR inhibitors led to an increase in lysosomal staining (Fig. 1*E*). Of note, cells treated with the S6 kinase 1 (S6K1) inhibitor PF-4708671 (Fig. 1*F*) or shcJUN-expressing cells (see Fig. 4*B*) did not depict increased LC3B II expression levels supporting a degree of specificity of the GSK3 and mTOR inhibitors in activation of the autophagy/lysosomal system. Altogether, our results indicate that GSK3 inhibition triggers both apoptosis and autophagy in the pancreatic cancer cell line PANC1.

We previously showed that prolonged inhibition of GSK3 activity failed to induce apoptosis in the human non-trans-

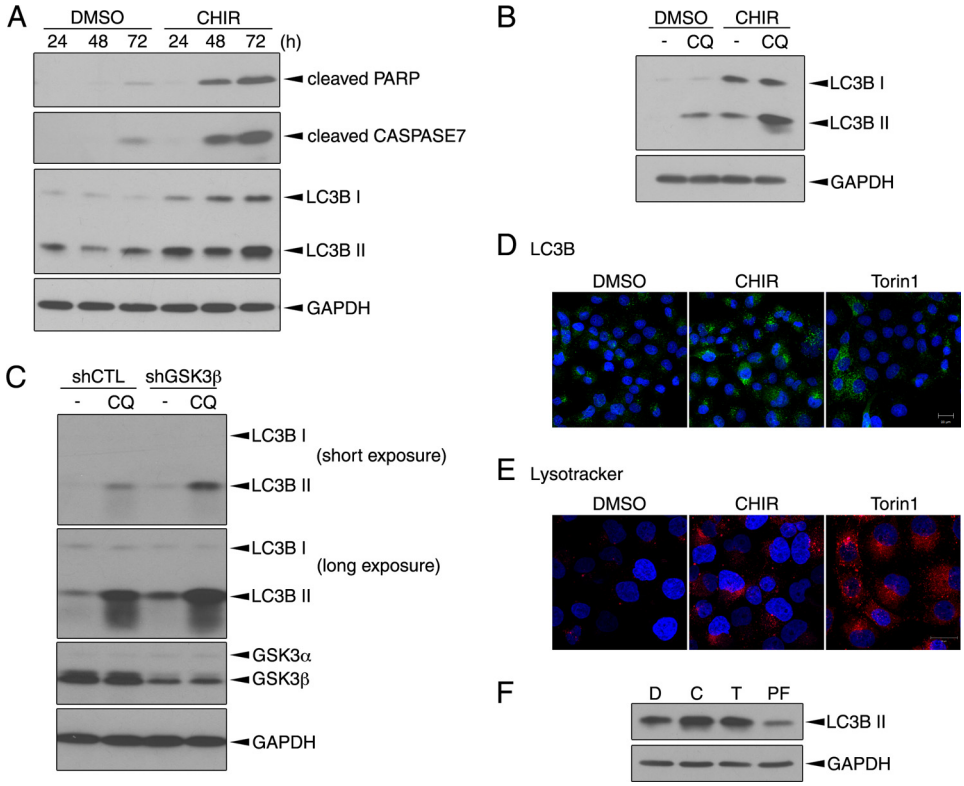

FIGURE 1. **Inhibition of GSK3 activity induces an autophagic response in human pancreatic cancer cells.** *A,* PANC1 cells were treated for the indicated time period with vehicle (DMSO) or GSK3 inhibitor CHIR99021 (CHIR; 5 μM). *B,* PANC1 cells were treated for 48 h with DMSO or CHIR99021 (CHIR; 5 μM). Chloroquine (*CQ*; 25 μM) was added or not (−) 4 h prior to cell lysis. *C,* PANC1 cells were infected with lentiviruses encoding either a non-targeting shRNA (shCTL) or a shGSK3β. 72 h post-infection, PANC1 cells were lysed after a 4-h incubation without (−) or with chloroquine (CQ; 25 μM). *A–C*, total cell lysates were analyzed by immunoblotting using the indicated antibodies. *D* and *E,* PANC1 cells were treated for 24 h with DMSO, CHIR99021 (*CHIR*; 5 μM), or the mTOR inhibitor Torin1 (250 nM). Autophagosome (punctate LC3B) (*D*) and lysosome (*E*) labeling was visualized with a Zeiss LSM700 confocal microscope. Images were acquired with a ×20 (*D*) or 63 (*E*) objective. Nuclei were stained with DAPI. *Scale bars*, 20 μm. *F*, PANC1 cells were treated for 48 h with vehicle (DMSO; *D*), GSK3 inhibitor CHIR99021 (*C*; 5 μM), mTOR inhibitor Torin1 (*T*; 250 nM), or S6K1 inhibitor PF-4708671 (*PF*; 20 μM). Total cell lysates were analyzed by immunoblotting using the indicated antibodies.

formed pancreatic epithelial cell line HPDE (8). To determine whether induction of autophagy was also specific to pancreatic cancer cells, HPDE cells were treated with CHIR99021 before assessing autophagy markers. Interestingly, increased expression levels of autophagosome membrane-bound LC3B II (Fig. 2*A*) and increased LC3B puncta staining were detected in HPDE cells upon treatment with GSK3 or mTOR inhibitor (Fig. 2*B*). These results suggest that the autophagic response induced upon GSK3 inhibition is not specific to pancreatic cancer cells but also applicable to non-transformed pancreatic epithelial cells. Of note, higher expression levels of LC3B II were observed in *Gsk3*$\beta^{-/-}$ immortalized MEF comparatively to *Gsk3*$\beta^{+/+}$ MEF (Fig. 2*C*).

Inhibition of Autophagy Sensitizes Human Pancreatic Cancer Cells to GSK3 Inhibition-induced Apoptosis—Given that various studies have suggested that autophagy may contribute to chemotherapeutic resistance by acting as a prosurvival mechanism (29–31, 37, 38), the role of autophagy in pancreatic cancer cell survival was addressed, particularly under conditions of GSK3 inhibition. Bafilomycin A1, a vacuolar H^+ ATPase inhibitor that prevents lysosome acidification, was used to inhibit autophagy. As previously reported (8), a 24-h treatment with GSK3 inhibitor failed to impact the expression of apoptotic markers, namely the cleavage of PARP and CASPASE 7 (Figs. 1*A* and 3*A*). However, concomitant treatment of cells with CHIR99021 and Bafilomycin A1 markedly promoted PARP and CASPASE 7 cleavage (Fig. 3*A*). Bafilomycin A1 also promoted PARP and CASPASE 7 cleavage in GSK3β-depleted cells (Fig. 3*B*), suggesting that inhibition of autophagy sensitizes pancreatic cancer cells to cell death upon GSK3 inhibition. To further validate the protective role of autophagy against GSK3 inhibition, autophagy was specifically inhibited by transfecting cells with a siRNA targeting ATG5, a protein involved in autophagosome formation (16, 17). The siRNA-mediated reduction in ATG5 was effective in blocking CHIR99021-induced LC3B II expression (Fig. 3*C*). Moreover, CHIR99021-treated cells transfected with a siATG5 displayed higher expression levels of cleaved PARP and CASPASE 7 (nearly 2-fold increase) compared with control cells transfected with a control siRNA. These data are consistent with a prosurvival role of autophagy following GSK3 inhibition. Soft-agarose assays were performed to confirm the impact of GSK3 and autophagy inhibition on pancreatic cancer cell growth. As previously published (8), treatment with GSK3 inhibitor impaired anchorage-independent growth by reducing the ability of PANC1 cells to form colonies in soft agarose by ~80% (Fig. 3*D*). Bafilomycin A1 was also effective in limiting anchorage-independent growth by 90%. The effect of the combined treatment of CHIR99021 and Bafilomycin A1 significantly differed from inhibitor treatment alone and was able to

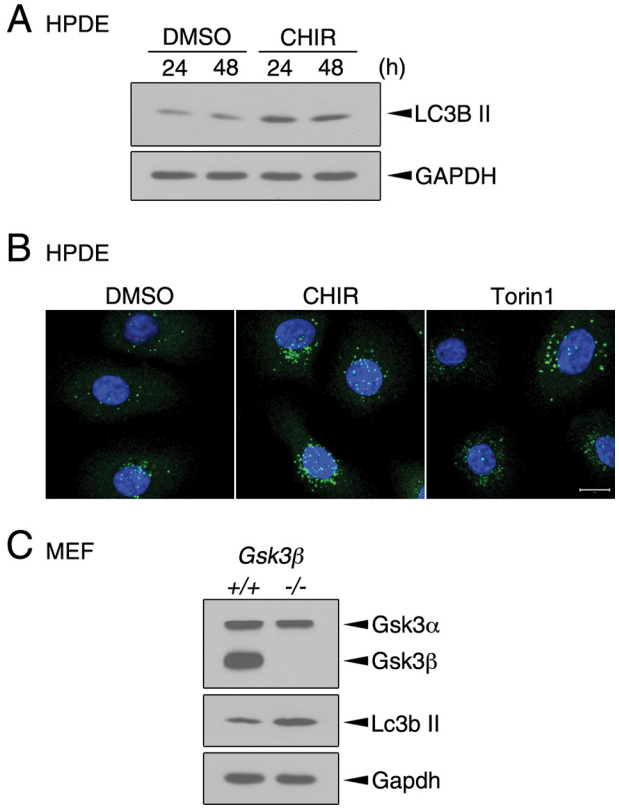

FIGURE 2. **Inhibition of GSK3 activity induces autophagy in non-transformed cells.** *A,* HPDE cells were treated for the indicated time with vehicle (DMSO) or CHIR99021 (*CHIR*; 5 μM). Total cell lysates were subjected to immunoblotting using the indicated antibodies. *B,* HPDE cells were treated for 24 h with DMSO, CHIR99021 (*CHIR*; 5 μM), or Torin1 (250 nM). Autophagosome (punctate LC3B) labeling was performed and nuclei were stained with DAPI. Stack images of 16–17 slices were acquired on a Zeiss LSM700 confocal microscope with a ×100 objective and the merged image is shown. *Scale bars*, 10 μm. *C,* exponentially growing *Gsk3β*$^{+/+}$ and *Gsk3β*$^{-/-}$ MEF were harvested and total cell lysates were analyzed by immunoblotting using the indicated antibodies.

almost completely abolish pancreatic cancer cell anchorage-independent growth (Fig. 3*D*).

We reported the requirement of JNK-cJUN pathway activation in GSK3 inhibition-mediated apoptosis (8). To identify the cellular and molecular mechanisms involved in the regulation of autophagy, the impact of JNK-cJUN inhibition on induced autophagy following GSK3 inhibitor treatment was assessed. Neither the JNK inhibitor SP600125 (Fig. 4*A*) nor shRNA-mediated cJUN down-regulation (Fig. 4*B*) was able to prevent CHIR99021-induced LC3B II expression, thereby excluding a major contribution of JNK-cJUN activity in the induction of autophagy following GSK3 inhibition. These results thus suggest that activation of the JNK-cJUN axis upon GSK3 inhibition is required for the apoptotic response (8) but dispensable for CHIR99021-induced autophagy.

Regulation of TFEB by GSK3 Inhibition—Our data revealed a potential impact of GSK3 inhibition on autophagosome and lysosomal biogenesis (Fig. 1). Recent studies identified TFEB as a master regulator of autophagy and lysosomal biogenesis (39, 40). Although the mechanisms controlling TFEB have not been extensively studied, it was nevertheless suggested that inhibition of mTORC1 links TFEB nuclear localization with autophagy and lysosomal biogenesis. In light of the above, subcellular TFEB localization was examined. As expected, a rapid nuclear translocation of TFEB was observed upon Torin1 treatment in HEK293T cells transiently transfected with an EGFP-fused TFEB (TFEB-EGFP) (Fig. 5*A*). A predominant nuclear localization of TFEB-EGFP was also detected in CHIR99021-treated HEK293T cells compared with DMSO-treated cells. Because the present experiments were mainly performed using pancreatic cancer cells, subcellular localization of TFEB was also assessed in PANC1 cells. Surprisingly, TFEB-EGFP staining was predominantly found in the nucleus of untreated (fully fed) PANC1 cells (Fig. 5*B*). To verify whether the latter represented an artifact of overexpression, the subcellular localization of endogenous TFEB was investigated. Confocal microscopy analysis enabled the confirmation of a predominant nuclear localization of TFEB in fully fed conditions (DMSO-treated) (Fig. 5*C*), with over 70% of PANC1 cells displaying nuclear labeling for TFEB (Fig. 5*D*). Despite this high percentage, both GSK3 and mTOR inhibitor treatment significantly increased the number of cells with nuclear TFEB staining (Fig. 5*D*) and further promoted the nuclear localization of TFEB (Fig. 5*E*). Of note, human non-transformed pancreatic epithelial HPDE cells displayed predominant cytoplasmic TFEB localization under normal conditions, whereas GSK3 inhibition led to enriched TFEB nuclear staining (Fig. 5*F*). Our data thus suggest that, likewise to mTOR inhibitor, treatment with GSK3 inhibitors promote TFEB nuclear localization.

Expression levels of TFEB were next investigated by immunoblotting. An acceleration of the electrophoretic mobility of endogenous TFEB was observed, particularly in the nuclear fraction, upon treatment of PANC1 cells with the GSK3 inhibitor CHIR99021 (Fig. 6*A*). Accordingly, shGSK3α/β-depleted cells displayed an acceleration of the electrophoretic mobility of TFEB (Fig. 6*B*). Treatment with Torin1 also modified the migration pattern of TFEB albeit to a lesser extent (Fig. 6, *A* and *C*). The alteration of TFEB migration on SDS-PAGE upon CHIR99021 treatment was comparable with that observed in HEK293T and in another pancreatic cancer cell line, namely MIA PaCa-2 (Fig. 6*C*). Another GSK3 inhibitor SB216763 was as potent as CHIR99021 in accelerating TFEB electrophoretic mobility (see Fig. 9*D*). Noteworthy, the GSK3 inhibitor-induced TFEB acceleration of electrophoretic mobility occurred without any significant impact on the activity of the mTORC1-S6K1 axis as measured by phosphorylation of the established mTORC1 substrate S6K1 (Fig. 6*C*). These results suggest that GSK3 inhibition modifies the post-translational profile of TFEB. Of note, preventing CHIR99021-induced autophagy (Fig. 3*C*) or caspases activation and PARP cleavage (Fig. 6*E*) did not alter the acceleration of TFEB electrophoretic mobility upon GSK3 inhibition (Fig. 6, *D* and *E*). These results suggest that detection of autophagy and apoptotic markers followed the impact of GSK3 inhibition on TFEB. Furthermore, autophagy induction appears independent of the apoptotic signals given that the caspase inhibitor was inefficient in blocking the CHIR99021-induced LC3B II expression (Fig. 6*E*).

To explain the above effect on TFEB mobility shift, a previous study suggested that a substantial fraction of TFEB is phosphorylated under fully fed conditions thereby contributing to its higher molecular weight size (41). Given that the impact on

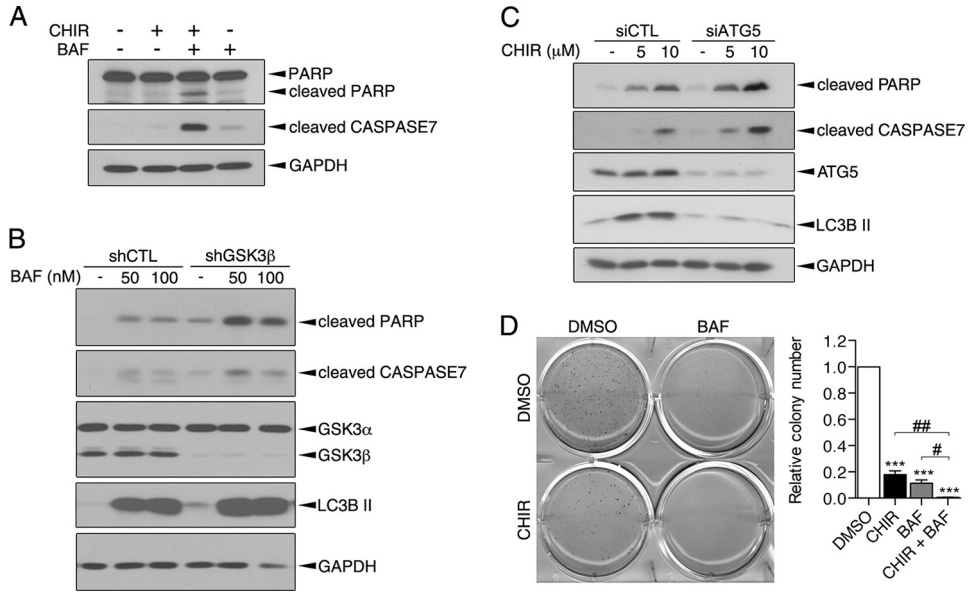

FIGURE 3. **Inhibition of autophagy sensitizes human pancreatic cancer cells to apoptosis upon GSK3 inhibition.** *A,* PANC1 cells were treated for 24 h with vehicle DMSO (−), CHIR99021 (*CHIR*; 5 μM), and/or Bafilomycin A1 (*BAF*; 50 nM). *B,* PANC1 cells were infected with lentiviruses encoding either a non-targeting shRNA (shCTL) or a shGSK3β. 48-h post-infection cells were treated with vehicle DMSO (−) or Bafilomycin A1 (*BAF*) for 24 h. *C*, PANC1 cells were transfected with either a control siRNA or siATG5. The following day, cells were treated with DMSO (−) or CHIR99021 (*CHIR*) for 48 h. *A-C*, total cell lysates were analyzed by immunoblotting using the indicated antibodies. *D,* PANC1 cells were seeded in soft-agarose and treated with DMSO, CHIR99021 (*CHIR*; 5 μM), and/or Bafilomycin A1 (*BAF*; 5 nM). After 3 weeks, colonies were stained with 3-(4,5-dimethylthiazol-2-yl)-2,5-diphenyltetrazolium bromide. Representative images of one experiment are shown. Colonies were counted using the ImageJ software and the number of colonies in control (DMSO-treated) was set at 1. A graphical representation of 3–5 independent experiments performed in duplicate is shown. ***, $p \leq 0.0001$ as compared with DMSO-treated cells. #, $p \leq 0.05$; ##, $p \leq 0.01$.

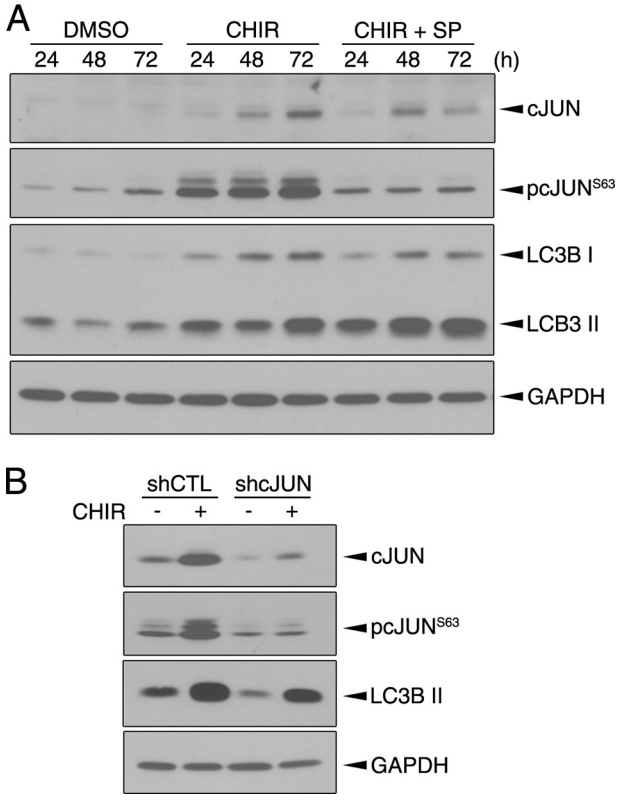

FIGURE 4. **JNK-cJUN activation is not required for the GSK3 inhibition-induced autophagy.** *A,* PANC1 cells were treated for the indicated time with vehicle DMSO, CHIR99021 (*CHIR*; 5 μM), and/or the JNK inhibitor SP600125 (*SP*; 25 μM). *B,* stable cell populations of PANC1-shCTL and PANC1-shcJUN were treated for 72 h with DMSO (−) or CHIR99021 (*CHIR*; 5 μM). *A* and *B*, total cell lysates were analyzed by immunoblotting using the indicated antibodies.

TFEB migration was evident as early as 30 min after CHIR99021 treatment, we tested whether GSK3 inhibition leads to TFEB dephosphorylation through the involvement of endogenous phosphatases. Cells were pre-treated with the serine/threonine phosphatase inhibitor Calyculin A. The increase in phosphorylation of ERK1/2, known to be highly regulated by phosphatases (42), was assessed to confirm phosphatase inhibition. Addition of Calyculin A prevented the CHIR99021-induced TFEB mobility shift (Fig. 7*A*) supporting a role for endogenous serine/threonine phosphatases in dephosphorylation of TFEB upon GSK3 inhibition. Calyculin A also prevented the Torin1-induced TFEB mobility shift. Dephosphorylation of TFEB on its Ser^{211}, corresponding to a consensus 14-3-3 binding site, has been associated with increased TFEB nuclear localization (41, 43). To test whether this phosphosite was affected by GSK3 inhibition, we immunoprecipitated TFEB and assessed Ser^{211} phosphorylation using a selective anti-phospho-Ser 14-3-3 binding motif as previously done by others (41, 44). Reduced phosphorylation levels of TFEB on its 14-3-3 binding motif, Ser^{211}, was observed upon GSK3 and mTOR inhibition (Fig. 7*B*). Collectively, the above data suggest that treatment with GSK3 and mTOR inhibitors leads to the dephosphorylation of TFEB, among others on its Ser^{211}, and promotes its nuclear localization.

Previous reports indicated that decreased TFEB phosphorylation following mTORC1 inhibition correlates with 14-3-3 dissociation from TFEB (41, 43). Co-immunoprecipitation studies confirmed the reduction in 14-3-3 interaction with TFEB upon Torin1 treatment in both HEK293T (Fig. 8*A*) and PANC1 cells (Fig. 8*B*). Similar results were obtained in CHIR99021-treated cells. Accordingly, quantitative mass spectrometry analysis

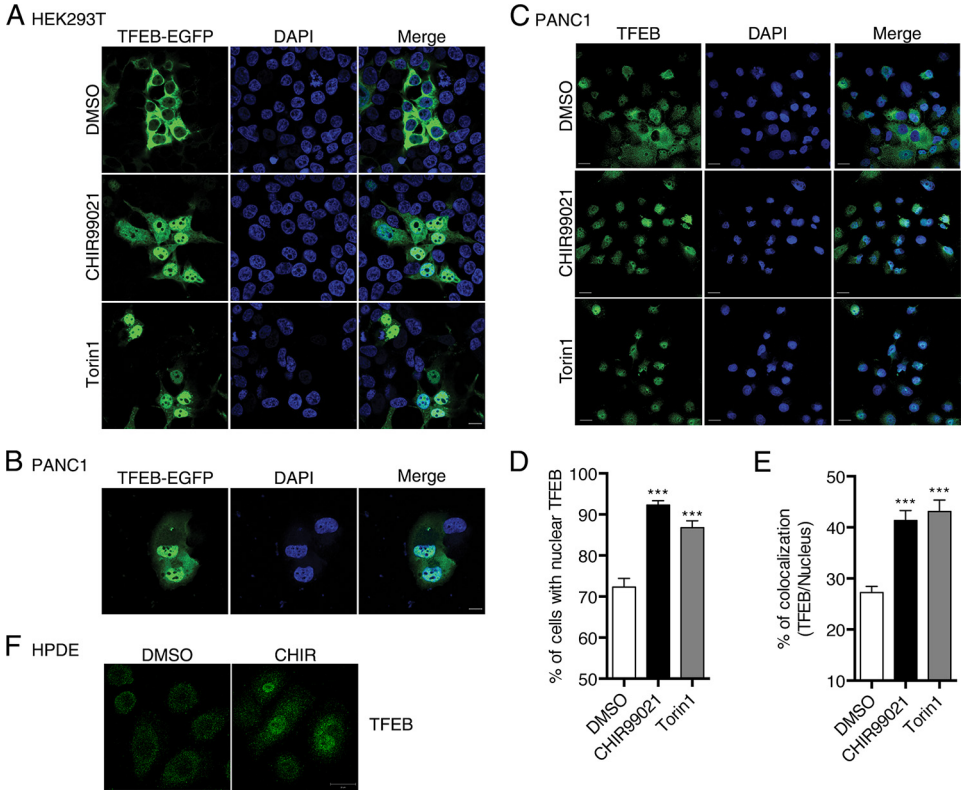

FIGURE 5. **GSK3 inhibition promotes TFEB nuclear localization.** *A* and *B,* confocal microscopy analysis of the subcellular distribution of the transfected TFEB-EGFP in HEK293T cells (*A*) and PANC1 (*B*) incubated 1 h (*A*) or not (*B*) with vehicle DMSO, CHIR99021 (5 μM), or Torin1 (250 nM). Nuclei were stained with DAPI. *Scale bars*, 10 μm. *C–E*, PANC1 cells were incubated for 1 h with vehicle DMSO, CHIR99021 (5 μM), or Torin1 (250 nM). Subcellular localization of the endogenous TFEB was analyzed by confocal microscopy using an antibody against TFEB. Nuclei were stained with DAPI. Representative micrographs are shown (*C*). *Scale bars*, 20 μm. *D*, quantification of the percentage of PANC1 cells with nuclear TFEB staining. *E*, quantification of the percentage of colocalization of TFEB with DAPI. ***, $p \leq 0.0001$ compared with DMSO-treated cells. *F*, confocal microscopy analysis of the subcellular distribution of TFEB in HPDE incubated 1 h with vehicle DMSO or CHIR99021 (*CHIR*; 5 μM). *Scale bars*, 20 μm.

demonstrated that five 14-3-3 proteins were highly associated with TFEB in DMSO-treated cells as denoted by their high M/L ratio. Upon CHIR99021 or Torin1 treatments, these 14-3-3 proteins were observed to be less associated with TFEB as revealed by the low H/M ratios (Fig. 8*C* and Table 1). Several histones and other nuclear proteins, although poorly interacting with TFEB in DMSO-treated cells, were detected and were among the most associated TFEB partners upon either CHIR99021 or Torin1 treatment (Fig. 8*C* and Table 1). Collectively, these results are in accordance with a dissociation of 14-3-3 proteins from TFEB followed by its nuclear translocation upon treatment with GSK3 and mTOR inhibitors.

The present data suggest that GSK3 inhibition, although promoting apoptosis also induces prosurvival signals, which may involve the participation of autophagy and/or TFEB. To address the possibility that the fostering of TFEB function contributes to the prosurvival signals induced by GSK3 inhibitors, a stable PANC1 population expressing a TFEB-targeting shRNA was generated. This PANC1-shTFEB population displayed lower expression levels of some autophagy and lysosomal markers such as BECLIN-1 and LAMP1 (Fig. 9*A*). Most importantly, reduced autophagic flux was observed in the PANC1-shTFEB population compared with the PANC1-shCTL population when treated with the GSK3 inhibitor CHIR99021 (Fig. 9*B*) suggesting that induction of autophagy is compromised in the PANC1-shTFEB population upon GSK3 inhibition. Noteworthy, the PANC1-shTFEB population displayed a reduced capacity to form colonies in soft agarose compared with the PANC1-shCTL population (Fig. 9*C*) suggesting that TFEB sustains PANC1 anchorage-independent growth. CHIR99021 was effective in limiting anchorage-independent growth of both PANC1-shCTL and PANC1-shTFEB cells. Additionally, PANC1 cells with reduced expression levels of TFEB were more sensitive to GSK3 inhibitor-induced apoptosis as visualized by the increased expression of cleaved PARP and CASPASE 7 (Fig. 9*D*). Torin1 treatment failed to impact these apoptotic markers, whether in PANC1-shCTL or PANC1-shTFEB cells. These findings suggest that TFEB limits apoptosis particularly when pancreatic cancer cells are treated with GSK3 inhibitors.

DISCUSSION

Our study defines a novel cellular process induced by GSK3 inhibitors in pancreatic cancer cells. In addition to triggering apoptotic signals (8), GSK3 inhibitors concomitantly elicit activation of the autophagy/lysosomal network. Interfering with this network sensitizes pancreatic cancer cells to GSK3 inhibitor-induced apoptosis suggesting the existence of prosurvival signals to counterbalance the death signals. Induction of autophagy has been observed in response to various chemotherapeutic agents in numerous cancer cells including pancreatic cancer cells (27–31, 37, 38). Because the present findings point toward a cytoprotective effect of autophagy in pancreatic

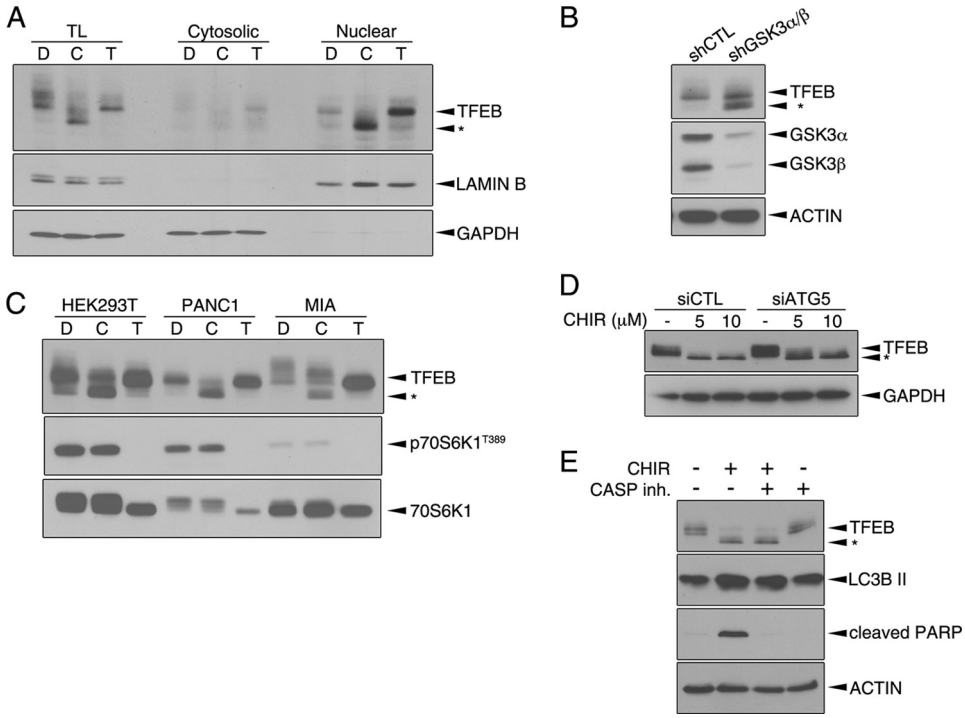

FIGURE 6. **GSK3 inhibition modifies TFEB electrophoretic mobility.** *A,* PANC1 cells were incubated for 1 h with vehicle DMSO (*D*), CHIR99021 (*C*; 5 μM), or Torin1 (*T*; 250 nM). Cytosolic and nuclear proteins were fractionated as described under "Experimental Procedures." Immunoblotting analyses of total cell lysates (*TL*), cytosolic and nuclear fractions were performed using the specified antibodies. *B,* PANC1 cells were infected with lentiviruses encoding either a non-targeting shRNA (shCTL) or a combination of shGSK3α and shGSK3β. Total cell lysates were prepared 72 h post-infection. *C,* HEK293T, PANC1, and MIA PaCa-2 (*MIA*) cells were treated 1 h with DMSO (*D*), CHIR99021 (*C*; 5 μM), or Torin1 (*T*; 250 nM). TFEB expression levels and S6K1 activity were analyzed by immunoblotting. *D,* PANC1 cells were transfected with either a control siRNA or siATG5. The following day, cells were treated with DMSO (−) or CHIR99021 (*CHIR*) for 24 h. *E,* PANC1 cells were treated for 48 h with vehicle DMSO (−), CHIR99021 (*CHIR*; 5 μM), and/or a *pan*-caspase inhibitor (*CASP inh.*; 10 μM). *B–E*, total cell lysates were analyzed by immunoblotting using the indicated antibodies. The *asterisk* (*) denotes the GSK3 inhibition-induced accelerated mobility shift of TFEB.

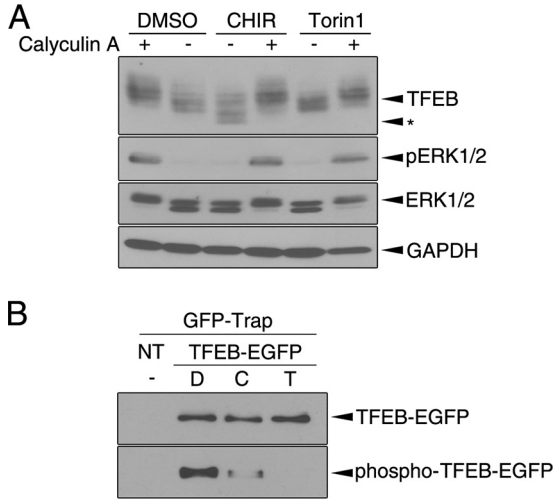

FIGURE 7. **GSK3 inhibition leads to the dephosphorylation of TFEB.** *A*, PANC1 cells were pre-treated (+) or not (−) for 15 min with Calyculin A (10 nM) followed by a 30-min incubation with DMSO, CHIR99021 (*CHIR*; 5 μM), or Torin1 (250 nM). Total cell lysates were analyzed by immunoblotting using the indicated antibodies. The *asterisk* (*) denotes the GSK3 inhibition-induced accelerated mobility shift of TFEB. *B,* HEK293T cells were transfected or not (*NT*) with the TFEB-EGFP expression vector. Twenty-four hours post-transfection, cells were treated for 1 h with vehicle DMSO (*D*), CHIR99021 (*C*; 5 μM), or Torin1 (*T*; 250 nM). Total cell lysates were prepared and TFEB-EGFP was immunoprecipitated using GFP-Trap-agarose beads followed by immunoblotting analyses of immunoprecipitates. TFEB-EGFP expression was analyzed using an anti-GFP antibody. Phosphorylation of TFEB-EGFP on Ser^{211} was analyzed using an anti-phospho-Ser 14-3-3 binding motif.

cancer cells, these observations potentially encourage the monitoring of autophagy when testing (new) chemotherapeutic agents. In particular, given that we and others have suggested testing GSK3 inhibitors in the setting of PDAC patients (5, 6, 8, 9, 11, 12, 45, 46), our results underscore the need to further explore the GSK3 downstream effectors to define better combination therapies. Concomitant GSK3 and autophagy inhibitors appear as an attractive new therapeutic option for PDAC patients given that such inhibitors, including lithium (47, 48) and chloroquine (49), have been safely used in clinical settings for many years. However, before going down that road, inactivation of GSK3 combined with autophagy and/or TFEB inhibition will require detailed investigation in *in vivo* settings using, as an example, mouse models of PDAC.

Few reports have proposed potential mechanisms for autophagy regulation by GSK3 (13–15). Noteworthy, in fully fed murine neuroblastoma cells, increased lysosomal biogenesis was observed upon Gsk3 inhibition although the underlying mechanism remained unclear (14). The present data are in line with these results as we observed increased LC3B II expression, autophagic flux, and/or lysosomal staining in fully fed GSK3-restricted pancreatic cancer cells, non-tumoral pancreatic epithelial cells and in MEF cells. Mechanistically, we were able to exclude a role of the JNK-cJUN axis in the induction of autophagy and rather suggest that apoptosis and autophagy signals generated upon GSK3 inhibitor treatment emanate from distinct effectors.

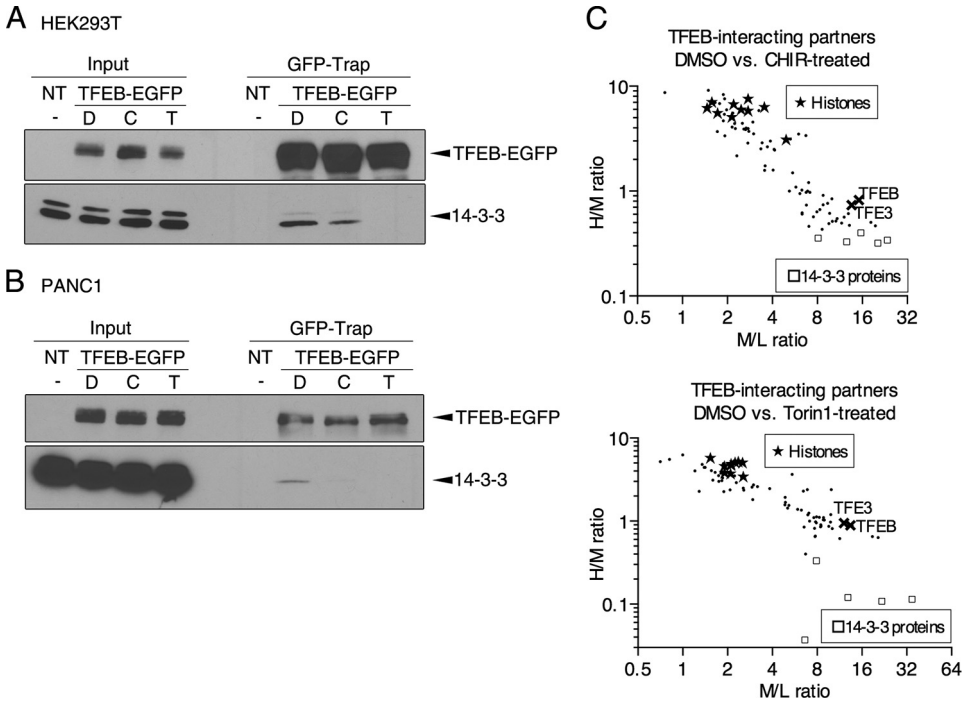

FIGURE 8. **GSK3 and mTOR inhibition modifies the profile of TFEB interacting partners.** *A* and *B,* HEK293T (*A*) and PANC1 (*B*) cells were transfected or not (*NT*) with the TFEB-EGFP expression vector. Twenty-four hours post-transfection, cells were treated for 1 h with vehicle DMSO (*D*), CHIR99021 (*C*; 5 μM), or Torin1 (*T*; 250 nM). Total cell lysates were prepared and TFEB-EGFP was immunoprecipitated using GFP-Trap-agarose beads followed by immunoblotting analyses of immunoprecipitates and their inputs. *C,* quantitative mass spectrometry analysis of medium (*M*) and heavy (*H*)-labeled HEK293T cells transfected with TFEB-EGFP compared with control (nontransfected) light (*L*)-labeled HEK293T. M-labeled HEK293T were treated for 1 h with DMSO (as control), whereas H-labeled HEK293T cells were treated with CHIR99021 (*CHIR*; 5 μM) (*top*) or Torin1 (250 nM) (*bottom*) for 1 h. Medium/light (M/L) ratios (enriched peptides in TFEB immunoprecipitates in control (DMSO-treated) cells) are plotted against heavy/medium (H/M) ratios (enriched peptides in TFEB immunoprecipitates following CHIR (*top*) or Torin1 (*bottom*) treatment). Only the top 20% M/L ratio peptides in both experiments and/or the top 20% H/M ratio peptides were plotted. For a complete list see Table 1.

Our study provides further support for a role of GSK3 in the regulation of TFEB, a recently identified master transcriptional regulator of autophagy and lysosomal biogenesis (40). A recent study in murine neuroblastoma cells has shown that Gsk3 inhibition leads to nuclear translocation of TFEB (14). Our data support such regulation although it remains unclear as to whether the nuclear translocation of TFEB represents the primary mode of regulation of TFEB upon GSK3 inhibition because a predominant nuclear TFEB localization was observed in fully fed PANC1 cells. Regardless of its subcellular localization in fully fed cells, we have still observed enrichment of nuclear TFEB correlating with its 14-3-3 dissociation upon GSK3 inhibition in both HEK293T and PANC1 cells suggesting that TFEB is subjected to similar GSK3-dependent regulation in different cell types. The reason for the enriched nuclear TFEB localization in fully fed PANC1 cells as opposed to the cytoplasmic TFEB localization in fully fed HEK293T and HPDE is unclear. Increased nuclear localization of the transcription factor E3, likewise to TFEB, a member of the MiTF/TFE transcription factor family, was observed in renal tumors from Birt-Hogg-Dubé syndrome patients, a syndrome associated with a germline mutation of the *FLCN* gene (50). Recent studies further supported a role for *FLCN* in the cytoplasmic retention of transcription factor E3, MiTF, and TFEB (51, 52). The status of the *FLCN* gene in PANC1 cells as well as its contribution to nuclear TFEB accumulation remain unknown, although testing of this avenue in the future could prove of valuable interest. Still, recent proteomic analyses have revealed an increased abundance of TFEB-regulated proteins specifically in human pancreatic cancer tissues compared with normal and chronic pancreatitis tissues (53), suggesting that TFEB may be particularly transcriptionally active (nuclear) in pancreatic cancer cells.

The majority of studies to date suggested that mTORC1-dependent phosphorylation of TFEB allowed its cytoplasmic retention and, logically, inhibition of mTORC1 activity was associated with non(less)-phosphorylated forms and nuclear accumulation of TFEB (41, 43, 44, 52, 54, 55). Notwithstanding the latter, we reasoned that dephosphorylation of TFEB within 30 min could not be explained by the sole preclusion of TFEB phosphorylation. Not only does the present data provide support for a role of endogenous serine/threonine phosphatases in the rapid dephosphorylation of TFEB, among others on its Ser^{211} upon treatment with GSK3 and mTOR inhibitors, but also show that the dephosphorylation events occurring on TFEB are under a strict regulatory process. From the experiments herein, it is clear that GSK3 and mTOR inhibition differently and independently impinge on the status of TFEB phosphorylation and it is our belief that GSK3 employs different means than those used by mTOR to impair TFEB phosphorylation. In support of this hypothesis, TFEB dephosphorylation and nuclear translocation were consistently observed upon GSK3 inhibition at a time point (30 – 60 min) at which no modulation in the activity of the mTORC1-S6K1 axis was observed. It is thus tempting to speculate that TFEB may be controlled by a panel of kinases and phosphatases that

TABLE 1

TFEB-interacting proteins identified by quantitative mass spectrometry

Medium (M) and heavy (H)-labeled HEK293T cells transfected with TFEB-EGFP compared to control (nontransfected) light (L)-labeled HEK293T. Medium (M)-labeled HEK293T cells were treated for 1 h with DMSO (as control), whereas heavy (H)-labeled HEK293T cells were treated with CHIR99021 (CHIR; 5 μM) or Torin1 (250 nM) for 1 h. The top 20% M/L ratio peptides in both experiments and/or the top 20% H/M ratio peptides were retrieved. These peptides were plotted on graphs as presented in Fig. 8*C*.

Protein names	DMSO- vs. CHIR-treated			DMSO- vs. Torin1-treated		
	M/L ratio	H/L ratio	H/M ratio	M/L ratio	H/L ratio	H/M ratio
TFEB-related proteins						
TFEB	15,184	17,134	0,82266	13,402	14,353	0,88795
TFE3	13,595	9,9861	0,73452	12,104	12,221	0,94742
14-3-3 proteins						
1433B	20,329	5,6695	0,31964	6,6082	0,24497	0,03707
1433E	15,649	5,8439	0,39887	12,899	1,7977	0,12041
1433G	8,1103	4,2809	0,35585	7,9009	3,5161	0,33363
1433T	12,582	5,4892	0,32745	34,718	3,8646	0,11425
1433Z	23,52	7,3233	0,34129	21,797	2,4882	0,1081
mTOR-associated proteins						
LTOR1	19,584	9,1423	0,46683	9,8883	11,161	1,1956
RRAGC;RRAGD	10,083	4,1719	0,51332	9,8381	9,229	0,97235
Histones						
H2AV;H2AZ	1,5731	11,583	7,0409	2,5257	13,631	5,0627
H2AY	1,7167	9,5412	5,5577	1,5331	8,8245	5,7559
H2AW	4,9367	15,321	3,1034	1,9068	8,5708	3,8186
H33;H32;H31T;H31;H32	2,7481	16,925	5,8319	2,1154	9,8653	4,8812
H12;H14;H13	2,1422	11,017	5,0847	2,0955	7,9971	3,7168
H2A1C;H2A3;H2A1B	1,4606	8,4739	6,1911	1,904	6,7226	4,601
H2A1J;H2A1H;H2AJ;H2A2C;H2A2A;H2A1D;H2A1;H2A1A;H2AX	3,5416	23,513	6,3322	2,5474	11,133	3,4254
H2B1L;H2B1M;H2B1N;H2B1H;H2B2F;H2B1C;H2B1D;H2BFS;H2B1K	2,2002	14,8	6,7266	2,3569	11,241	5,2126
H4	2,4706	14,857	5,9811	2,1112	10,126	4,7289
ADT3	7,5234	4,356	0,56728	8,4427	7,0862	0,85485
H2B3B;H2B2E;H2B1B;H2B1O;H2B1J;H2B2D;H2B2C	2,7487	19,866	7,596	2,2462	10,648	5,0788
Other DNA binding proteins						
ILF2	4,1131	9,9592	2,5025	2,5675	6,8603	2,3547
ILF3	1,9214	6,2985	3,3727	2,9851	8,0486	2,7386
MBB1A	6,3054	6,4341	1,0204	4,8579	7,6123	1,567
PARP1	6,0032	20,568	3,4978	5,4314	19,786	3,6597
RUVB2	3,5561	5,5943	1,5732	6,2623	9,0543	1,3579
SAFB1	3,3554	10,022	2,5278	2,5478	6,4437	2,5018
SMCA5;SMCA1	3,4122	9,4471	2,8828	3,8431	9,4838	2,4645
SMC1A	3,878	11,117	3,0003	9,9432	24,185	2,3941
SSRP1	4,1389	10,291	2,4605	2,9177	7,6053	2,5627
SP16H	3,6996	9,5218	2,645	3,1747	8,3543	2,6042
TOP1	1,9126	12,731	7,564	0,81589	4,5246	5,5456
TOP2A	1,7147	8,7889	3,6962	2,4806	9,2042	3,416
TOP2B	2,2394	9,8738	4,4092	2,1143	8,1883	3,6068
XRCC5	6,6927	21,365	3,3741	6,4516	14,942	2,3026
XRCC6	5,2712	14,648	3,132	6,8665	18,02	2,3922
RNA binding proteins						
ACINU	2,1521	12,49	4,0689	1,8278	9,1867	3,8738
C1QBP	10,011	8,0852	0,84123	8,9342	9,1941	1,0291
ELAV1	2,9944	10,704	3,5107	1,8876	5,2795	2,2616
FBRL	1,8821	8,8219	4,6872	1,7443	6,1478	3,5246
ROA1;RA1L2	2,1744	13,717	5,5332	1,3913	5,0463	4,4215
ROA2	1,772	10,327	6,8194	1,2072	5,2115	4,0219
ROA3	1,9062	9,1252	5,3835	1,6468	6,6824	3,8701
ROAA	2,7487	10,843	3,9447	1,8219	7,1302	4,0133
HNRPC;HNRCL	1,9774	11,423	5,9649	1,4125	6,8976	4,4215
HNRPD	2,9558	14,377	4,5496	1,5547	6,596	4,0609
HNRPF	4,0515	6,5069	1,5838	4,894	8,0905	1,6826
HNRH3	1,881	15,67	8,3303	1,5949	5,2481	3,1211
HNRPL	2,6476	8,2139	3,8577	2,2867	4,6985	2,8974
HNRPM	2,5192	11,283	4,4182	1,8009	6,616	3,7898
HNRPU	2,7423	8,5586	2,8686	2,0803	5,2321	2,376
HNRDL	3,2497	15,661	5,869	1,8488	6,0921	3,3127
MATR3	2,5745	9,6038	3,9101	2,1821	6,3547	3,472
PABP2	2,3167	5,0111	2,163	2,2289	8,2011	3,5103
PININ	2,2569	9,0217	3,9442	1,2884	2,9364	2,279
RBMX;RMXL1	2,7883	11,079	3,7076	1,831	5,2941	3,0629
SF3B1	3,5809	7,1414	1,7416	4,8678	9,1056	1,9322
Nuclear envelope-associated proteins						
CBX3	2,6658	10,603	3,9908	1,7476	5,0731	3,0066
EMD	9,5528	4,6412	0,49093	11,36	7,1647	0,61573
LMNB1	1,6546	10,821	6,9617	1,8732	8,9432	4,9346
LAP2B	8,6178	1,7508	0,43067	6,6962	2,6932	0,40219
Cytoskeleton-associated proteins						
ACTS;ACTC;ACTH;ACTA	0,76151	8,2948	8,7147	0,70693	3,9913	5,2114
VIME	1,4891	12,669	9,1256	0,99931	6,7551	6,2603
Transporters						
ABCD3	6,3287	4,1783	0,62055	8,4882	6,8938	0,87344
ADT2	10,847	5,4295	0,54821	10,097	8,3164	0,81453
CMC2	7,0257	3,5732	0,46102	7,8919	7,5468	0,95626
DIC	7,9325	5,1823	0,63455	7,9417	9,3752	1,1236
M2OM	8,3306	5,9737	0,66768	7,8097	8,0295	0,97743
TXTP	6,339	3,2571	0,60354	7,1102	7,4484	1,0008
Heat Shock proteins						
CH60	10,628	6,2748	0,51755	7,6829	6,2683	0,81641
GRP78	9,6834	6,1899	0,61207	7,7835	4,9314	0,66162
HSP7C	12,896	7,3597	0,61072	13,737	11,489	0,87532
HSP71	18,286	9,7192	0,50444	18,812	12,347	0,65164
HSP76;HSP70B	11,612	5,4528	0,49533	7,741	5,0249	0,65044
Ribosomal proteins						
RL10	8,7379	7,5749	0,91035	8,847	9,6436	1,1023
RL13A	5,2034	5,4019	0,99812	5,0646	7,6878	1,4343
RL17	6,1073	6,3189	0,94425	8,2784	9,1831	1,1093
RL23	5,7467	6,7143	1,0899	7,6029	8,4258	1,1006
RL24	9,3817	7,0229	0,76501	8,8004	8,9815	1,0349
RL3	7,0063	7,3258	1,2073	5,1738	8,5651	1,5446
RS2	8,7625	6,3809	0,73953	8,4637	7,772	0,90415
RS24	7,1366	6,6993	0,9739	5,9214	8,2466	1,3855
RS27;RS27L	6,745	6,4512	0,73356	6,5365	5,5823	0,84456
RS6	6,892	7,7316	1,0022	7,0398	9,0105	1,2486
RS9	6,7277	6,4108	0,97419	6,9326	7,8472	1,1886
WDR43	0,94018	11,061	11,764	1,3475	6,4898	4,8163
Other proteins						
AK6	12,113	5,545	0,56482	20,56	14,77	0,63323
ECHA	13,125	6,1912	0,47171	9,5948	9,4701	0,86726
FLOT1	5,457	8,1406	1,4918	2,9568	5,3623	1,8135

respond to different environmental cues. To date, data from quantitative proteomics have identified over 19 phosphorylation sites on human TFEB (56–59). It is likely that several kinases and phosphatases are involved the regulation of these phosphosites. Although not directly tested in the current study, assessing the direct phosphorylation of TFEB by GSK3 should also prove of interest in future studies delineating the exact contribution of GSK3, as compared with mTOR, in TFEB regulation.

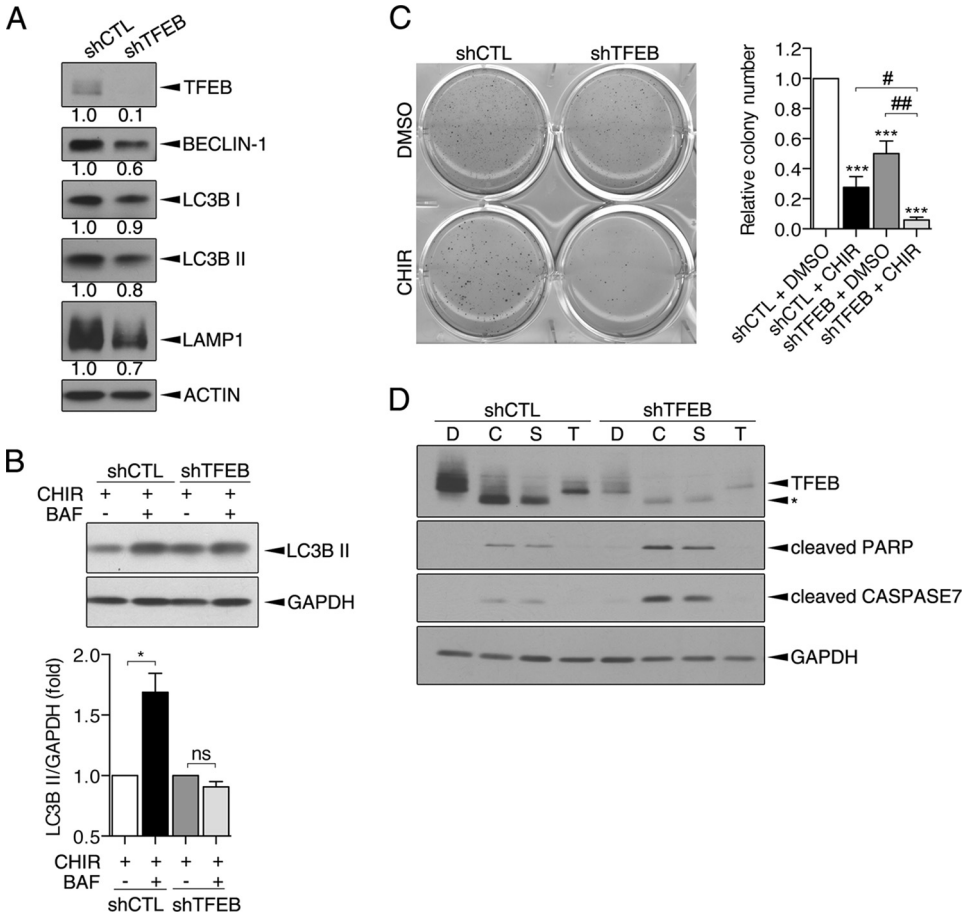

FIGURE 9. **TFEB knockdown sensitizes pancreatic cancer cells to apoptosis upon GSK3 inhibition.** *A*, total cell lysates from stable populations of PANC1-shCTL and PANC1-shTFEB were analyzed by immunoblotting using the indicated antibodies. *B,* stable populations of PANC1-shCTL and PANC1-shTFEB cells were treated for 48 h with CHIR99021 (*CHIR*; 5 μM). Bafilomycin A1 (*BAF*; 50 nM) was added or not (−) 4 h prior to cell lysis. LC3B II and GAPDH expression levels were analyzed by immunoblotting. Representative immunoblots are shown. A graphical representation of LC3B II/GAPDH expression levels where the ratio in cells untreated with Bafilomycin A1 was set at 1 is shown. *, $p \leq 0.05$. *ns* = not significant. *C,* stable populations of PANC1-shCTL and PANC1-shTFEB cells were seeded in soft-agarose, cultured for 3 weeks in the presence of DMSO or CHIR99021 (*CHIR*; 5 μM), colonies were stained and counted. Representative images of one experiment are shown. A graphical representation of 4 independent experiments performed in duplicate is shown. The number of colonies in PANC1-shCTL was set at 1. ***, $p \leq 0.001$ as compared with shCTL, DMSO-treated cells; #, $p \leq 0.05$; ##, $p \leq 0.01$. *D*, stable populations of PANC1-shCTL and PANC1-shTFEB cells were treated for 48 h with DMSO (*D*), GSK3 inhibitors CHIR99021 (*C*; 5 μM) or SB216763 (*S*; 20 μM), or Torin1 (*T*; 250 nM). Total cell lysates were analyzed by immunoblotting using the indicated antibodies. The *asterisk* (*) denotes the GSK3 inhibitor-induced accelerated mobility shift of TFEB.

Irrespective of the differential impact on TFEB phosphorylation, the present results globally support a positive contribution of GSK3 and mTOR inhibitors on TFEB transcriptional function. 14-3-3 dissociation from TFEB was previously proposed to unmask nuclear localization signals thereby promoting the nuclear localization of TFEB essential to the expression of its target genes (41). Our results support these observations given the observed loss of interaction of TFEB with 14-3-3 chaperones and TFEB nuclear accumulation upon treatment with GSK3 and mTOR inhibitors. To our knowledge, the present data are the first to perform a broad analysis of TFEB interacting partners in fully fed cells *versus* mTOR-restricted cells. Our findings also demonstrate an increased association of TFEB with transcriptional regulators upon mTOR inhibition. This increased association was similarly observed in GSK3-inhibited cells suggesting that both mTOR and GSK3 inhibition are associated with the promotion of TFEB nuclear function.

The present study provides evidence that TFEB contributes to the transformed phenotype of pancreatic cancer PANC1 cells because reduction of its expression impaired PANC1 anchorage-independent growth. The mechanism underlying this effect is, however, unknown. Studies assessing whether the reduced TFEB levels impinge on the high basal autophagy of human pancreatic cancer cells thereby altering their metabolism would be of particular interest. Indeed, it has previously been suggested that constitutive autophagy in pancreatic cancer cells enables their growth by sustaining oxidative phosphorylation thereby providing bioenergetic intermediates to various metabolic pathways (37). This potential role of TFEB in ensuring the proper metabolism of transformed cells may particularly predominate in metabolically restrictive conditions such as those observed when cells are grown in soft agarose. Our study is thus the first to unveil an important role of TFEB in the maintenance of the transformed phenotype of human pancreatic cancer cells. A recent study revealed an aberrant increase in the *N*-glycosylation of proteins regulated by TFEB in pancreatic cancer tissues (53) supporting a potential role for TFEB in pancreatic carcinogenesis. In other systems such as renal cell carcinoma and melanoma, TFEB, as well as its family members transcription factor E3 and MiTF, were proposed to display

oncogenic activity although the mechanisms involved remain elusive (60). One possibility emanating from the present work is that TFEB could operate by limiting apoptosis under specific stress conditions such as GSK3 inhibition.

In conclusion, the present study highlights a dual role for GSK3 in pancreatic cancer cell survival and strengthens the view that GSK3 is central in managing downstream signaling pathways involved in the regulation of pancreatic cancer cell growth. Unbalancing the activity of a GSK3 downstream effector could have a considerable impact on the decision of the cell to undergo cell death. It is possible that the accessibility of GSK3 effectors may explain the pleiotropic and context-dependent effect of GSK3 inhibitors. The present findings also raise innovative clues with regard to the role and regulation of TFEB. Herein, we demonstrate that endogenous phosphatases and kinases regulate directly or indirectly TFEB and that GSK3 inhibition leads to TFEB dephosphorylation, which correlates with TFEB dissociation from 14-3-3 chaperones and TFEB nuclear localization. A key finding of the present study is the demonstration that, under fully fed conditions, TFEB displays an aberrant nuclear localization in human pancreatic cancer PANC1 cells compared with the cytoplasmic TFEB in non-transformed pancreatic epithelial HPDE cells and that TFEB depletion significantly impairs PANC1 anchorage-independent growth suggesting an important role for TFEB in pancreatic cancer cell growth.

Acknowledgments—We are grateful to M. S. Tsao (University of Toronto, Canada) and J. R. Woodgett (The Lunenfeld-Tanenbaum Research Institute, Canada) for providing the HPDE and MEF cell lines, respectively. We thank S. M. Ferguson (Yale University School for Medicine) for the pEGFP-N1-TFEB construct (Addgene plasmid 38119). We thank P. Pothier for critical reading of the manuscript.

Note Added in Proof—In the version of this article that was published on January 5, 2015 as a Paper in Press, the blot image in Fig. 1*C* was not correct. The image in the original version represented a Western blot for LC3B in cells expressing an shRNA that did not target GSK3β as stated in the legend. The corrected version of Fig. 1*C* represents results with LC3B in cells expressing the correct shRNA that does target GSK3β.

REFERENCES

1. Bardeesy, N., and DePinho, R. A. (2002) Pancreatic cancer biology and genetics. *Nat. Rev. Cancer* **2,** 897–909
2. Hezel, A. F., Kimmelman, A. C., Stanger, B. Z., Bardeesy, N., and Depinho, R. A. (2006) Genetics and biology of pancreatic ductal adenocarcinoma. *Genes Dev.* **20,** 1218–1249
3. Schneider, G., Siveke, J. T., Eckel, F., and Schmid, R. M. (2005) Pancreatic cancer: basic and clinical aspects. *Gastroenterology* **128,** 1606–1625
4. Jones, S., Zhang, X., Parsons, D. W., Lin, J. C., Leary, R. J., Angenendt, P., Mankoo, P., Carter, H., Kamiyama, H., Jimeno, A., Hong, S. M., Fu, B., Lin, M. T., Calhoun, E. S., Kamiyama, M., Walter, K., Nikolskaya, T., Nikolsky, Y., Hartigan, J., Smith, D. R., Hidalgo, M., Leach, S. D., Klein, A. P., Jaffee, E. M., Goggins, M., Maitra, A., Iacobuzio-Donahue, C., Eshleman, J. R., Kern, S. E., Hruban, R. H., Karchin, R., Papadopoulos, N., Parmigiani, G., Vogelstein, B., Velculescu, V. E., and Kinzler, K. W. (2008) Core signaling pathways in human pancreatic cancers revealed by global genomic analyses. *Science* **321,** 1801–1806
5. Bang, D., Wilson, W., Ryan, M., Yeh, J. J., and Baldwin, A. S. (2013) GSK-3α promotes oncogenic KRAS function in pancreatic cancer via TAK1-TAB stabilization and regulation of noncanonical NF-κB. *Cancer Discov.* **3,** 690–703
6. Kitano, A., Shimasaki, T., Chikano, Y., Nakada, M., Hirose, M., Higashi, T., Ishigaki, Y., Endo, Y., Takino, T., Sato, H., Sai, Y., Miyamoto, K., Motoo, Y., Kawakami, K., and Minamoto, T. (2013) Aberrant glycogen synthase kinase 3β is involved in pancreatic cancer cell invasion and resistance to therapy. *PloS One* **8,** e55289
7. Mamaghani, S., Patel, S., and Hedley, D. W. (2009) Glycogen synthase kinase-3 inhibition disrupts nuclear factor-κB activity in pancreatic cancer, but fails to sensitize to gemcitabine chemotherapy. *BMC Cancer* **9,** 132
8. Marchand, B., Tremblay, I., Cagnol, S., and Boucher, M. J. (2012) Inhibition of glycogen synthase kinase-3 activity triggers an apoptotic response in pancreatic cancer cells through JNK-dependent mechanisms. *Carcinogenesis* **33,** 529–537
9. Ougolkov, A. V., Fernandez-Zapico, M. E., Savoy, D. N., Urrutia, R. A., and Billadeau, D. D. (2005) Glycogen synthase kinase-3β participates in nuclear factor κB-mediated gene transcription and cell survival in pancreatic cancer cells. *Cancer Res.* **65,** 2076–2081
10. Wilson, W., 3rd, and Baldwin, A. S. (2008) Maintenance of constitutive IκB kinase activity by glycogen synthase kinase-3α/β in pancreatic cancer. *Cancer Res.* **68,** 8156–8163
11. Miyashita, K., Nakada, M., Shakoori, A., Ishigaki, Y., Shimasaki, T., Motoo, Y., Kawakami, K., and Minamoto, T. (2009) An emerging strategy for cancer treatment targeting aberrant glycogen synthase kinase 3β. *Anticancer Agents Med. Chem.* **9,** 1114–1122
12. Zhang, J. S., Herreros-Villanueva, M., Koenig, A., Deng, Z., de Narvajas, A. A., Gomez, T. S., Meng, X., Bujanda, L., Ellenrieder, V., Li, X. K., Kaufmann, S. H., and Billadeau, D. D. (2014) Differential activity of GSK-3 isoforms regulates NF-κB and TRAIL- or TNFα induced apoptosis in pancreatic cancer cells. *Cell Death Dis.* **5,** e1142
13. Lin, S. Y., Li, T. Y., Liu, Q., Zhang, C., Li, X., Chen, Y., Zhang, S. M., Lian, G., Ruan, K., Wang, Z., Zhang, C. S., Chien, K. Y., Wu, J., Li, Q., Han, J., and Lin, S. C. (2012) GSK3-TIP60-ULK1 signaling pathway links growth factor deprivation to autophagy. *Science* **336,** 477–481
14. Parr, C., Carzaniga, R., Gentleman, S. M., Van Leuven, F., Walter, J., and Sastre, M. (2012) Glycogen synthase kinase 3 inhibition promotes lysosomal biogenesis and autophagic degradation of the amyloid-β precursor protein. *Mol. Cell. Biol.* **32,** 4410–4418
15. Yang, J., Takahashi, Y., Cheng, E., Liu, J., Terranova, P. F., Zhao, B., Thrasher, J. B., Wang, H. G., and Li, B. (2010) GSK-3β promotes cell survival by modulating Bif-1-dependent autophagy and cell death. *J. Cell Sci.* **123,** 861–870
16. Boya, P., Reggiori, F., and Codogno, P. (2013) Emerging regulation and functions of autophagy. *Nat. Cell. Biol.* **15,** 713–720
17. Lamb, C. A., Yoshimori, T., and Tooze, S. A. (2013) The autophagosome: origins unknown, biogenesis complex. *Nat. Rev. Mol. Cell Biol.* **14,** 759–774
18. Rabinowitz, J. D., and White, E. (2010) Autophagy and metabolism. *Science* **330,** 1344–1348
19. Strohecker, A. M., and White, E. (2014) Autophagy promotes BrafV600E-driven lung tumorigenesis by preserving mitochondrial metabolism. *Autophagy* **10,** 384–385
20. Guo, J. Y., Karsli-Uzunbas, G., Mathew, R., Aisner, S. C., Kamphorst, J. J., Strohecker, A. M., Chen, G., Price, S., Lu, W., Teng, X., Snyder, E., Santanam, U., Dipaola, R. S., Jacks, T., Rabinowitz, J. D., and White, E. (2013) Autophagy suppresses progression of K-ras-induced lung tumors to oncocytomas and maintains lipid homeostasis. *Genes Dev.* **27,** 1447–1461
21. Rosenfeldt, M. T., O'Prey, J., Morton, J. P., Nixon, C., MacKay, G., Mrowinska, A., Au, A., Rai, T. S., Zheng, L., Ridgway, R., Adams, P. D., Anderson, K. I., Gottlieb, E., Sansom, O. J., and Ryan, K. M. (2013) p53 status determines the role of autophagy in pancreatic tumour development. *Nature* **504,** 296–300
22. Yue, Z., Jin, S., Yang, C., Levine, A. J., and Heintz, N. (2003) Beclin 1, an autophagy gene essential for early embryonic development, is a haploinsufficient tumor suppressor. *Proc. Natl. Acad. Sci. U.S.A.* **100,** 15077–15082
23. Liang, X. H., Jackson, S., Seaman, M., Brown, K., Kempkes, B., Hibshoosh, H., and Levine, B. (1999) Induction of autophagy and inhibition of tumorigenesis by beclin 1. *Nature* **402,** 672–676

24. Liu, E. Y., and Ryan, K. M. (2012) Autophagy and cancer: issues we need to digest. *J. Cell Sci.* **125,** 2349–2358
25. Guo, J. Y., Chen, H. Y., Mathew, R., Fan, J., Strohecker, A. M., Karsli-Uzunbas, G., Kamphorst, J. J., Chen, G., Lemons, J. M., Karantza, V., Coller, H. A., Dipaola, R. S., Gelinas, C., Rabinowitz, J. D., and White, E. (2011) Activated Ras requires autophagy to maintain oxidative metabolism and tumorigenesis. *Genes Dev.* **25,** 460–470
26. Yang, S., Wang, X., Contino, G., Liesa, M., Sahin, E., Ying, H., Bause, A., Li, Y., Stommel, J. M., Dell'antonio, G., Mautner, J., Tonon, G., Haigis, M., Shirihai, O. S., Doglioni, C., Bardeesy, N., and Kimmelman, A. C. (2011) Pancreatic cancers require autophagy for tumor growth. *Genes Dev.* **25,** 717–729
27. Mukubou, H., Tsujimura, T., Sasaki, R., and Ku, Y. (2010) The role of autophagy in the treatment of pancreatic cancer with gemcitabine and ionizing radiation. *Int. J. Oncol.* **37,** 821–828
28. Pardo, R., Lo Ré, A., Archange, C., Ropolo, A., Papademetrio, D. L., Gonzalez, C. D., Alvarez, E. M., Iovanna, J. L., and Vaccaro, M. I. (2010) Gemcitabine induces the VMP1-mediated autophagy pathway to promote apoptotic death in human pancreatic cancer cells. *Pancreatology* **10,** 19–26
29. Hashimoto, D., Bläuer, M., Hirota, M., Ikonen, N. H., Sand, J., and Laukkarinen, J. (2014) Autophagy is needed for the growth of pancreatic adenocarcinoma and has a cytoprotective effect against anticancer drugs. *Eur. J. Cancer* **50,** 1382–1390
30. Papademetrio, D. L., Cavaliere, V., Simunovich, T., Costantino, S., Campos, M. D., Lombardo, T., Kaiser, C. M., and Alvarez, E. (2013) Interplay between autophagy and apoptosis in pancreatic tumors in response to gemcitabine. *Target. Oncol.* **9,** 123–134
31. Donohue, E., Thomas, A., Maurer, N., Manisali, I., Zeisser-Labouebe, M., Zisman, N., Anderson, H. J., Ng, S. S., Webb, M., Bally, M., and Roberge, M. (2013) The autophagy inhibitor verteporfin moderately enhances the antitumor activity of gemcitabine in a pancreatic ductal adenocarcinoma model. *J. Cancer* **4,** 585–596
32. Furukawa, T., Duguid, W. P., Rosenberg, L., Viallet, J., Galloway, D. A., and Tsao, M. S. (1996) Long-term culture and immortalization of epithelial cells from normal adult human pancreatic ducts transfected by the E6E7 gene of human papilloma virus 16. *Am. J. Pathol.* **148,** 1763–1770
33. Ouyang, H., Mou, Lj., Luk, C., Liu, N., Karaskova, J., Squire, J., and Tsao, M. S. (2000) Immortal human pancreatic duct epithelial cell lines with near normal genotype and phenotype. *Am. J. Pathol.* **157,** 1623–1631
34. Hoeflich, K. P., Luo, J., Rubie, E. A., Tsao, M. S., Jin, O., and Woodgett, J. R. (2000) Requirement for glycogen synthase kinase-3β in cell survival and NF-κB activation. *Nature* **406,** 86–90
35. Boisvert, F. M., Ahmad, Y., Gierlinski, M., Charriere, F., Lamont, D., Scott, M., Barton, G., and Lamond, A. I. (2012) A quantitative spatial proteomics analysis of proteome turnover in human cells. *Mol. Cell. Proteomics* **11,** M111.011429
36. Zhou, J., Tan, S. H., Nicolas, V., Bauvy, C., Yang, N. D., Zhang, J., Xue, Y., Codogno, P., and Shen, H. M. (2013) Activation of lysosomal function in the course of autophagy via mTORC1 suppression and autophagosome-lysosome fusion. *Cell Res.* **23,** 508–523
37. Yang, S., and Kimmelman, A. C. (2011) A critical role for autophagy in pancreatic cancer. *Autophagy* **7,** 912–913
38. Maes, H., Rubio, N., Garg, A. D., and Agostinis, P. (2013) Autophagy: shaping the tumor microenvironment and therapeutic response. *Trends Mol. Med.* **19,** 428–446
39. Settembre, C., Di Malta, C., Polito, V. A., Garcia Arencibia, M., Vetrini, F., Erdin, S., Erdin, S. U., Huynh, T., Medina, D., Colella, P., Sardiello, M., Rubinsztein, D. C., and Ballabio, A. (2011) TFEB links autophagy to lysosomal biogenesis. *Science* **332,** 1429–1433
40. Settembre, C., Fraldi, A., Medina, D. L., and Ballabio, A. (2013) Signals from the lysosome: a control centre for cellular clearance and energy metabolism. *Nat. Rev. Mol. Cell Biol.* **14,** 283–296
41. Roczniak-Ferguson, A., Petit, C. S., Froehlich, F., Qian, S., Ky, J., Angarola, B., Walther, T. C., and Ferguson, S. M. (2012) The transcription factor TFEB links mTORC1 signaling to transcriptional control of lysosome homeostasis. *Sci. Signal.* **5,** ra42
42. Owens, D. M., and Keyse, S. M. (2007) Differential regulation of MAP kinase signalling by dual-specificity protein phosphatases. *Oncogene* **26,** 3203–3213
43. Martina, J. A., Chen, Y., Gucek, M., and Puertollano, R. (2012) MTORC1 functions as a transcriptional regulator of autophagy by preventing nuclear transport of TFEB. *Autophagy* **8,** 903–914
44. Martina, J. A., and Puertollano, R. (2013) Rag GTPases mediate amino acid-dependent recruitment of TFEB and MITF to lysosomes. *J. Cell Biol.* **200,** 475–491
45. Garcea, G., Manson, M. M., Neal, C. P., Pattenden, C. J., Sutton, C. D., Dennison, A. R., and Berry, D. P. (2007) Glycogen synthase kinase-3β: a new target in pancreatic cancer? *Curr. Cancer Drug Targ.* **7,** 209–215
46. Billadeau, D. D. (2007) Primers on molecular pathways: the glycogen synthase kinase-3β. *Pancreatology* **7,** 398–402
47. Martinez, A. (2008) Preclinical efficacy on GSK-3 inhibitors: towards a future generation of powerful drugs. *Med. Res. Rev.* **28,** 773–796
48. Cohen, P., and Goedert, M. (2004) GSK3 inhibitors: development and therapeutic potential. *Nat. Rev. Drug Disc.* **3,** 479–487
49. Lee, S. J., Silverman, E., and Bargman, J. M. (2011) The role of antimalarial agents in the treatment of SLE and lupus nephritis. *Nat. Rev. Nephrol.* **7,** 718–729
50. Hong, S. B., Oh, H., Valera, V. A., Baba, M., Schmidt, L. S., and Linehan, W. M. (2010) Inactivation of the FLCN tumor suppressor gene induces TFE3 transcriptional activity by increasing its nuclear localization. *PloS One* **5,** e15793
51. Martina, J. A., Diab, H. I., Lishu, L., Jeong-A., L., Patange, S., Raben, N., and Puertollano, R. (2014) The nutrient-responsive transcription factor TFE3 promotes autophagy, lysosomal biogenesis, and clearance of cellular debris. *Sci. Signal.* **7,** ra9
52. Petit, C. S., Roczniak-Ferguson, A., and Ferguson, S. M. (2013) Recruitment of folliculin to lysosomes supports the amino acid-dependent activation of Rag GTPases. *J. Cell Biol.* **202,** 1107–1122
53. Pan, S., Chen, R., Tamura, Y., Crispin, D. A., Lai, L. A., May, D. H., McIntosh, M. W., Goodlett, D. R., and Brentnall, T. A. (2014) Quantitative glycoproteomics analysis reveals changes in *N*-glycosylation level associated with pancreatic ductal adenocarcinoma. *J. Proteome Res.* **13,** 1293–1306
54. Efeyan, A., Zoncu, R., Chang, S., Gumper, I., Snitkin, H., Wolfson, R. L., Kirak, O., Sabatini, D. D., and Sabatini, D. M. (2013) Regulation of mTORC1 by the Rag GTPases is necessary for neonatal autophagy and survival. *Nature* **493,** 679–683
55. Settembre, C., Zoncu, R., Medina, D. L., Vetrini, F., Erdin, S., Erdin, S., Huynh, T., Ferron, M., Karsenty, G., Vellard, M. C., Facchinetti, V., Sabatini, D. M., and Ballabio, A. (2012) A lysosome-to-nucleus signalling mechanism senses and regulates the lysosome via mTOR and TFEB. *EMBO J.* **31,** 1095–1108
56. Olsen, J. V., Vermeulen, M., Santamaria, A., Kumar, C., Miller, M. L., Jensen, L. J., Gnad, F., Cox, J., Jensen, T. S., Nigg, E. A., Brunak, S., and Mann, M. (2010) Quantitative phosphoproteomics reveals widespread full phosphorylation site occupancy during mitosis. *Sci. Signal.* **3,** ra3
57. Dephoure, N., Zhou, C., Villén, J., Beausoleil, S. A., Bakalarski, C. E., Elledge, S. J., and Gygi, S. P. (2008) A quantitative atlas of mitotic phosphorylation. *Proc. Natl. Acad. Sci. U.S.A.* **105,** 10762–10767
58. Chen, R. Q., Yang, Q. K., Lu, B. W., Yi, W., Cantin, G., Chen, Y. L., Fearns, C., Yates, J. R., 3rd, and Lee, J. D. (2009) CDC25B mediates rapamycin-induced oncogenic responses in cancer cells. *Cancer Res.* **69,** 2663–2668
59. Kettenbach, A. N., Schweppe, D. K., Faherty, B. K., Pechenick, D., Pletnev, A. A., and Gerber, S. A. (2011) Quantitative phosphoproteomics identifies substrates and functional modules of Aurora and Polo-like kinase activities in mitotic cells. *Sci. Signal.* **4,** rs5
60. Haq, R., and Fisher, D. E. (2011) Biology and clinical relevance of the micropthalmia family of transcription factors in human cancer. *J. Clin. Oncol.* **29,** 3474–3482